SPE-211538-MS

Technical Feasibility of a Through Tubing Circumferential Zonal Isolation Gamma Scanner for Plug and Abandonment Implementations

Feyzi Inanc, Allan Jones, Peng Yuan, and Toyli Anniyev, Baker Hughes; Johan Kverneland, TotalEnergies EP Norge; Pierre Chuilon, TotalEnergies SE

Copyright 2022, Society of Petroleum Engineers DOI 10.2118/211538-MS

This paper was prepared for presentation at the ADIPEC held in Abu Dhabi, UAE, 31 October – 3 November 2022.

This paper was selected for presentation by an SPE program committee following review of information contained in an abstract submitted by the author(s). Contents of the paper have not been reviewed by the Society of Petroleum Engineers and are subject to correction by the author(s). The material does not necessarily reflect any position of the Society of Petroleum Engineers, its officers, or members. Electronic reproduction, distribution, or storage of any part of this paper without the written consent of the Society of Petroleum Engineers is prohibited. Permission to reproduce in print is restricted to an abstract of not more than 300 words; illustrations may not be copied. The abstract must contain conspicuous acknowledgment of SPE copyright.

Abstract

This paper presents a feasibility study of a novel nuclear sensor design toward finding volumetric flaws in cement behind two or more tubulars in a wellbore. The sensor concept targets plug and abandonment activities and the presented results include experimental test setups built for the purpose, results of simulations and experiments conducted for determining the range of applicability.

The measurement is based on a gamma-gamma measurement concept that incorporates a rotating interrogating beam illuminating the wellbore for an azimuthal scan while the tool is in motion in the borehole. The radiation source is a conventional Cs-137 radioisotope emitting 662 keV gamma rays that can penetrate through two metallic tubulars to reach the cement. The detector is a gamma detector that is collimated to accept gamma rays from the volume illuminated with the gamma rays and centrally positioned in the tool body. The detector collimator rotates in synchronization with the rotating interrogating beam providing an azimuthal scanning capability.

The feasibility of the concept was initially tested through simulations that provided encouraging results for detection of volumetric flaws in the cement between the outer casing and the formation. This was followed by experiments that were conducted using synthetic test formations embedded with various volumetric cement flaws. The rock sizes were representative of infinite rocks encountered in typical logging runs. The experimental setup provided not only different flaw sizes but also different tubing positions inside the casing annulus. A generic gamma-gamma tool was run vertically in the synthetic rocks without a tubing and with a tubing in place. The vertical runs were repeated around the borehole and images were formed. Another mode of experiment was conducted by rotating the tool around its axis. The motivation behind this was to study the azimuthal response of the gamma-gamma scanner in an eccentered position. The results from the experiments were in line with the simulation results confirming that it is possible to detect volumetric flaws in the cement between the outer casing and the formation.

This paper demonstrates a method for detecting cement flaws that is pivotal in plug and abandonment activities. Different measurement techniques are usually sensitive to different flaw morphologies. While nuclear methods cannot detect micro-channeling, they can be very efficient in detecting volumetric flaws in cement. In contrast, such flaws cannot be efficiently detected by other measurement techniques. The results

presented here show how a gamma-gamma measurement can be used to detect and characterize volumetric cement flaws that can be encountered in multi-annular completions.

Introduction

Properly abandoning some of the oil wells have become an important activity with the aging of some of the oil reservoirs. One common practice in the industry is to plug these aging wells so that there would not be a communication between the surface and different layers in the well and pollution concern is kept at check. This is usually enforced by the various governmental regulations so that operators make significant investments to ensure that this abandonment process is done properly.

An important step in the abandonment process is to characterize the state of the cement behind the casing. Most cement flaws can be traced back to cementing process (Mwang'ande 2016). A plug in the wellbore does not provide the required isolation unless any issues in the cement are fixed. There has been significant efforts and technology development toward determining such cement problems in the past. The cement bond logs have been available for that purpose for a long time (Pilkington and Fertl, 1975, Gollwitzer and Masson, 1982). Even recent LWD tools started to deploy pulse-echo ultrasonic transducers for imaging the casing and cement around it (Hawtorn, A, Steinsiek, R, Rahman, Shaela, 2022). Although sonic methods have found widespread application for the cement characterization in single casing wells, doing the same in a multistring completion is more challenging. One approach for remedying this is to pull the tubing from the well and then use the conventional sonic approach for evaluating the cement. This usually requires significant investment in time and cost. Therefore, industry has a desire for technologies that can provide the same cement evaluation with the tubing in place.

One alternative in cement characterization through multistring completions is to use nuclear methods because neutron and gamma radiation can penetrate through the multiple strings and reach the cement. While this is an advantage with the nuclear methods, they also come with some disadvantages. Nuclear inspection methods are usually sensitive to volumetric changes. Therefore, detection of microannulus outside the casing is usually a challenge for nuclear methods since microannulus is layer type flaw rather than a volumetric flaw. In contrast, nuclear methods are more promising for cement channeling type flaws due to their volumetric morphology. One nuclear method for cement quality and flaw interrogation in the cased environments is using a Cs-137 gamma source as the interrogating beam and measuring the gamma rays scattered from the completion materials and formation. There has been some work in the past and recent times where the open hole density measurements were repurposed for cased hole density measurements (Moake 1998, Ellis, et al., 2004, Li, et al., 2022). Although the target of those measurements was determination of the formation density measurement, they are close to the general principle of the measurements used in this study where the measurement target is the cement flaw inspection in the multistring completions. An example of such a measurement is given in the paper by Kasten and et al. (Kasten, et al., 2016). Also, there are simulation based studies in literature for cement evaluation in single string cases (Yike, et al., 2016).

The main focus of the work presented here is to perform cement evaluation measurements in multistring completions with azimuthal sensitivity. For that reason, we have developed a gamma ray scanner concept with a rotating interrogating beam and rotating shield around a centralized detector (Inanc et al., 2021). Although the tool prototype is in the development phase, measurement concept has been tested using existing slick density tools in test fixtures specifically designed for the cement evaluation purposes. The test fixtures included different size cement flaws with the capability of moving the tubing into different positions. The liquid volume in front of the density tool faces is known to have a large influence on the measurements. The assessment of this was the motivation why tubing movement capability was introduced into the test fixtures. The measurements included both static and dynamic measurements where the tool was moving vertically and tool was rotating around its own axis. The results from the experiments were in line with the

simulation results confirming that it is possible to detect volumetric flaws in the cement between the outer casing and the formation. Some of the results from the rotating tool experiments showed the importance of the liquid volume in front of the detectors and we have developed an approach for mitigating this affect to increase the detectability of the cement flaws where the tubing in the annulus is not centralized.

Background

Although the proposed conceptual design has similarities to the gamma-gamma density measurements, it also differs from those in an important aspect. In a typical open hole wireline implementation, we are concerned with the gamma transport only in the formation. In the LWD measurements, we may have some borehole fluid in front of the tool face. Some LWD implementations provide density measurements with a standoff between the tool face and the formation, but some others make use of the data only when the tool face is in contact with the formation similar to wireline implementations. But in either case wireline or LWD, we do not have high atomic number and high-density elements such as casing iron in the volume of interrogation. In short, the typical open hole density measurements are engaged with material that has elements ranging from oxygen (Z=8) to calcium (Z=20). While there may be some low atomic number hydrogen and carbon present in the formation, their magnitude is lower compared to the typical formation elements. In contrast, any measurement in a multistring cased hole environment will face not only the formation material but it will need to account for high atomic number elements in the casings and low effective atomic number brines and muds present in the annuli. The presence of such high atomic number element environment and low atomic number element environment is what differs the proposed gamma ray scanner measurements from conventional gamma-gamma measurements.

The challenges with a gamma ray scanner in the cased hole environment can be discussed using Figures 1 and 2. Figure 1 shows the photoelectric absorption and incoherent scattering cross sections cross over energy values. The low atomic number group of materials such as brines and lighter weight muds will typically include elements that are going to be lower than Z=8 and plot in Figure 1 tells us that gamma rays in that atomic number range will have a very large energy range where incoherent Compton scattering dominates the system. As it will be seen later, this group of materials will have a low gamma ray absorption resulting in higher count rates reported by the detectors. The second group where the atomic numbers range from 8 to 20 are still Compton scattering dominated region, but photoelectric absorption cross sections play a larger role. This can easily be seen if the region between the 0-energy point to blue separation line is compared to the region between the blue separation line and the green line showing the Cs-137 emission energy value. As this comparison shows, the first segment is larger compared to the first segment in the 1-7 atomic number region. This second group will provide count rates much lower than the first group material count rates since there is a higher absorption cross section involved. The third group is for the region where the atomic number $Z > 20$. If we compare the left side of the blue line to the right side, we see that there is a much larger photoelectric absorption activity there that will result in very low count rates. The comparison of those 3 groups of materials can also be seen in Figure 2 (XCOM, 2010). The bottom green curve is for water with very low interaction cross sections. The intermediate curves are for limestone and sandstone and they overlap after about 0.15 MeV. That is pretty much the reason why gamma-gamma density measurements are relatively lithology insensitive. The top one is for iron and it is significantly higher compared to the others and this drives the significant drop in the count rates.

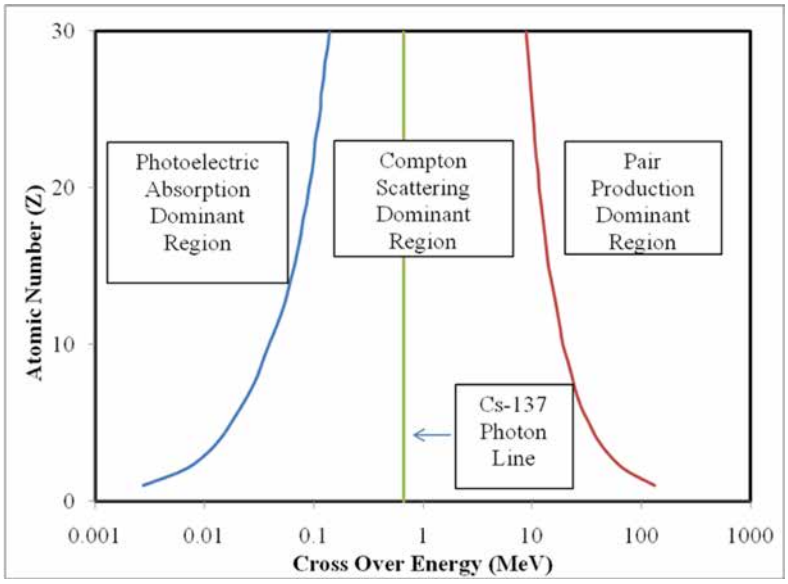


Figure 1—Photoelectric Absorption and Compton Scattering Cross Sections Cross Over Energy Values as a Function of Atomic Number.

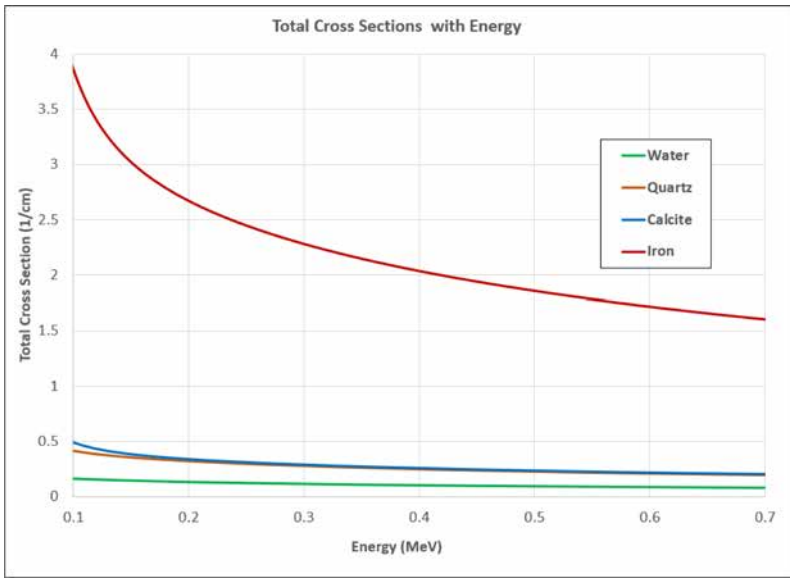


Figure 2—Total Cross Sections for Water, Sandstone, Limestone and Iron as a Function of Gamma Ray Energy

This comparison of three groups of materials involved with cased whole implementations shows why cased hole implementations are different and more challenging. While a tool should accommodate very high count rates in presence of low atomic number and low density brines, it should also be able to collect enough count rates for reasonable measurements in presence of iron in the cased hole environments. For multiple string cases which is the focal point of this paper, the proposed tool will be facing varying amount of brine and casing as it travels in the wellbore and it should be able to accommodate rapidly varying count rates and this makes the measurement optimization quite challenging.

Gamma Ray Scanner Concept

The gamma ray scanner concept is based on a rotating beam and rotating detector window idea (Inanc, F et al., 2021). There is a high density high atomic number shield that surrounds both the detector and the source port. There is a window across from the detector and that window is coupled with the source

collimator that rotates together with the shield. With that we have a gamma ray beam interrogating the completion in an azimuthal manner and the detector accepting the incoming gamma rays that are synched with the source collimator. The detector window is adjustable for performing measurements with different azimuthal resolution levels. The concept is shown in the Figure 3. The shield is rotated through a motor and the incoming gamma rays are recorded together with the azimuthal position of the shield around the detector and the source to form an image of the borehole. The detector is a centralized detector to ensure that there is no azimuthal bias in the tool response. The results given in this work are meant to show the feasibility of this concept.

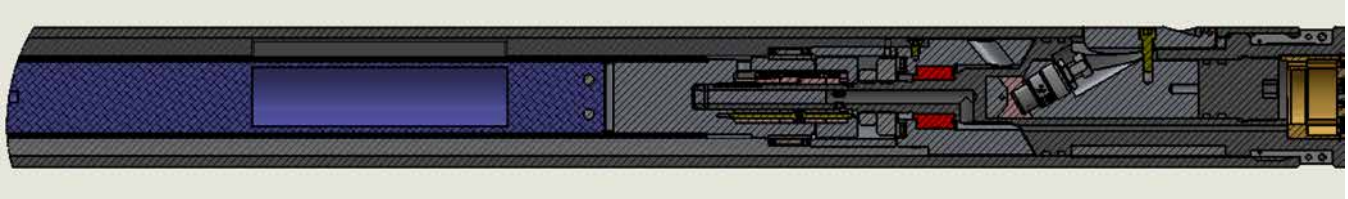


Figure 3—The Schematic Drawing of the Gamma Ray Imager Tool Concept.

Proof of Concept Simulations

The first step in the gamma scanner feasibility study was to perform simulations to see if we can prove the concept and if there was a merit in pushing forward with the experimental work that is usually costly and slow. For that, we have used Monte Carlo code MCNP (Werner, et al., 2018) where we modeled for a slick design wireline density tool that has the basics of a gamma scanner concept. The density tools deploy Cs-137 chemical sources and typically two gamma detectors. Usually, the short space detectors are about 20.0 cm away from the source and they are very sensitive to the borehole features and data from those detectors is used for correcting the density values provided by the long space detectors. The long space detectors are typically positioned about 40.0 cm away from the Cs-137 source and larger than the short space detectors to compensate the count rate losses due to the distance and additional attenuation compared to the short space detectors. The source to detector distance may show variability due to the design criteria of the companies building those.

Figure 4 shows the flaw morphology used in the simulations and experiments. There are 4 configurations in the plot. The left most one has the tool with red pressure housing placed inside a yellow tubing. The green fluid in the tubing is water. The green fluid outside the tubing is water again and it is surrounded by a thicker yellow casing region. Lighter green area outside the casing is cement and outermost region is the formation. As it moves from the left to the right, we see a darker green water region in the cement in the order of increasing size. The completion in the simulations is based on 4.0/4.5″ tubing, 6.0/7.0″ casing and 8.5″ borehole size. The flaw sizes are 0, 10, 20 and 30 degrees. The flaws have been designed as a pie shape with the degree referring to the angle between the upper and lower brackets of the pie used to define a flaw. Flaws are filled with water.

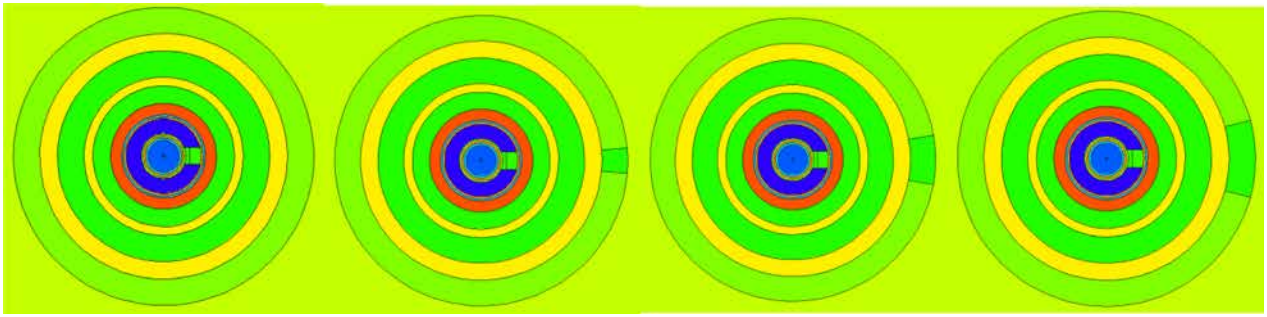


Figure 4—Flaw Size Morphology Used in the Proof-of-Concept Simulations

The simulations have been performed for 3 tubing positions shown in Figure 5. The tool face is very close to the casing material in the right eccentered case where the count rates should be lower. For the left eccentered case, there is a large volume of water in front of the tool face and the count rates should go up for that configuration. There are two sets of simulation data, one for short space detector simulations and the other is for long space detectors. Figure 6 shows the gamma ray spectra computed for the right eccentered, centered and left eccentered position and each plot has data for 0, 10, 20 and 30 degree flaw sizes. As the left most plot in Figure 6 shows, we see an increasing trend in the count rates computed through the simulations. That agrees with the physics of the problem briefly discussed in the background section where we showed that when there is a low density and low atomic number fluid in the system count rates increase. Since we have water in the flaw volume and water volume increases with the flaw size, the increasing count rate trend is in agreement with the physics. Another noticeable trend is the count rates increases as we go from the right eccentered to left eccentered positions. This increase comes with significant increase in the volume of water in front of the tool face as shown in Figure 5. The plots in Figure 7 shows the percent relative increases in the count rates compared to the no flaw cases. While the right eccentered tubing position provide some change up to 22%, the centered tubing case shows a sensitivity of 1.75% and no change in the left eccentered position. When factoring in the real world count rate statistics, it is clear that short space detector can sense a cement flaw only if the cement flaw is large and the tool face is pressed to where the flaw is. In short, we don't see an acceptable level of cement flaw sensitivity from short space detector data.

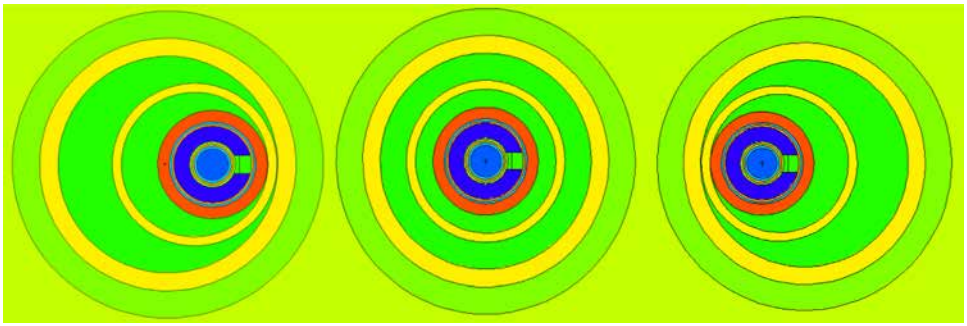


Figure 5—Tubing and Tool Positioning Used in the Simulations, Right Eccentered, Centered and Left Eccentered Sequentially.

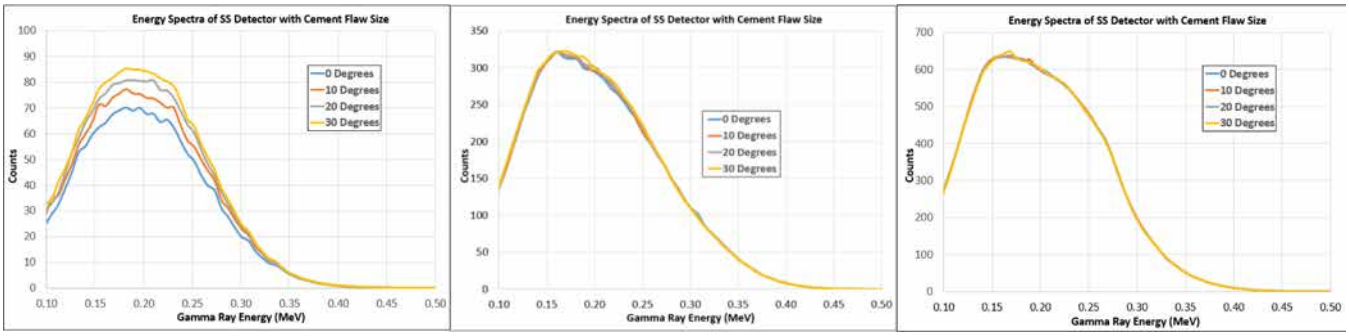


Figure 6—Short Space Detector Simulated Gamma Ray Spectra for Different Flaw Sizes for Right Eccentered, Centered and Left Eccentered Positions.

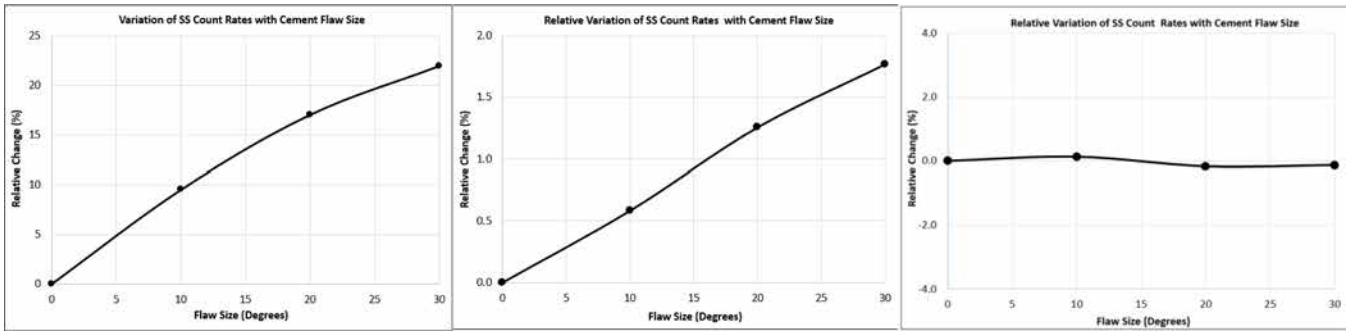


Figure 7—Relative Change in the Short Space Detector Count Rates with the Tubing Positioning and the Flaw Sizes.

The second set of data is from the long space detector simulations. Figure 8 shows the spectra from the long space detector for different tool and tubing positioning and flaw sizes. The general behavior of the long space spectra are similar to what we have observed with the short space detector. In this case, count rates increase with increasing flaw size more rapidly compared to the short space one. This is very visible when the long space right eccentered data is compared to short space right eccentered data. In addition, we see long space spectral counts increasing both in the centered and left eccentered positions that were not observed short space data.

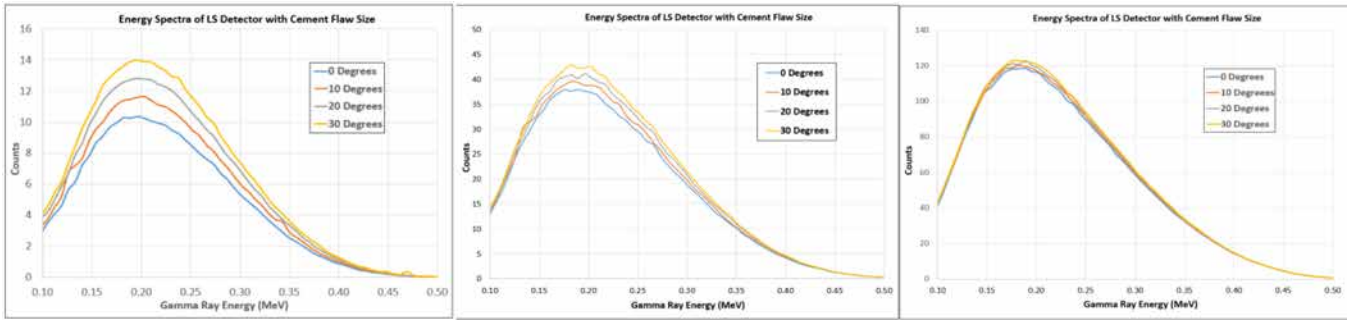


Figure 8—Long Space Detector Simulated Gamma Ray Spectra for Different Flaw Sizes for Right Eccentered, Centered and Left Eccentered Tubing Positions.

Figure 9 shows the percent relative change in the count rates for the long space detector in the same order used in the previous plots. For the right eccentered positioning, the maximum relative change goes up to 36%. This compares very favorably to the short space detector values that only go up to 22%. While the short space detector relative increases are very low and in the noise level, we do see count rate increases for the long space detector in the centered positioning that are likely to go out of noise region if the flaw

size 20 degrees and larger. For the left eccentered position, we may have difficulties with the sensitivities unless we log very slow and collect high precision data.

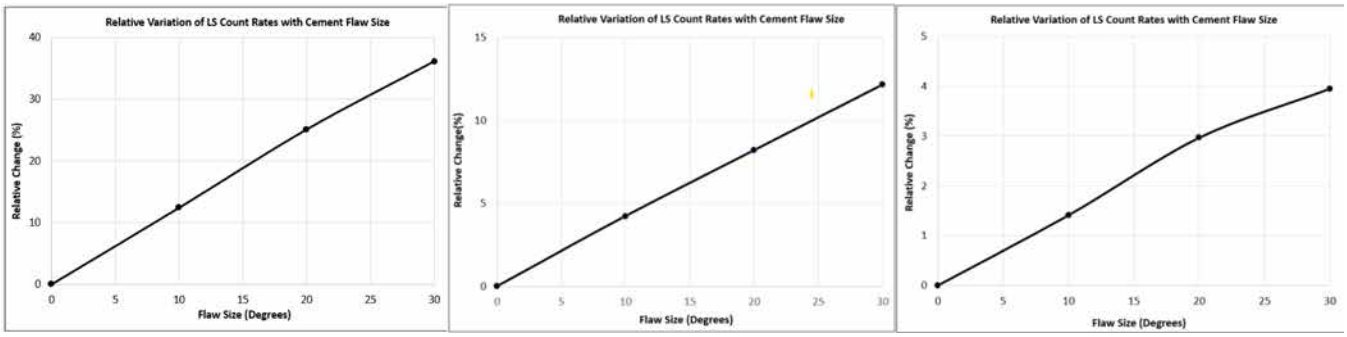


Figure 9—Relative Change in the Long Space Detector Count Rates with the Tubing Positioning and the Flaw Sizes.

One important outcome of this simulation based proof of concept study is that the gamma scanner concept should be able to detect the cement flaws in the multistring completions although the sensitivity decreases with increasing distance between the tool face and the flaw location.

Experimental Setups

For performing experiments, we built two synthetic rocks that had built in cement flaws. One was designed for gamma-gamma measurements with relatively thin formation thickness levels although they are still infinite thickness due to relatively shallow depth of investigation of 662 keV gamma rays. Gamma-gamma fixture in Figure 10 shows the radial and axial cross sections of the fixture. The dimensions of the fixture is 21″×21×72″. The cement between the casing and the outer material is class G cement used in the oil field. The casing OD and ID are 7.0″ and 6.0″. The tubing is a 4.50″ OD and 4.0″ ID tubing. The borehole size is 8.25″. The tubing position in the annulus can be adjusted to simulate right eccentered, centered and left eccentered tubing positions used in the proof-of-concept simulations. While the wall thickness may be small at certain directions, it is still an infinite rock because the depth of investigation of 662 keV gamma rays is relatively shallow in general, the tool is distanced from the formation and there is also significant amount of iron between the tool and the formation material.

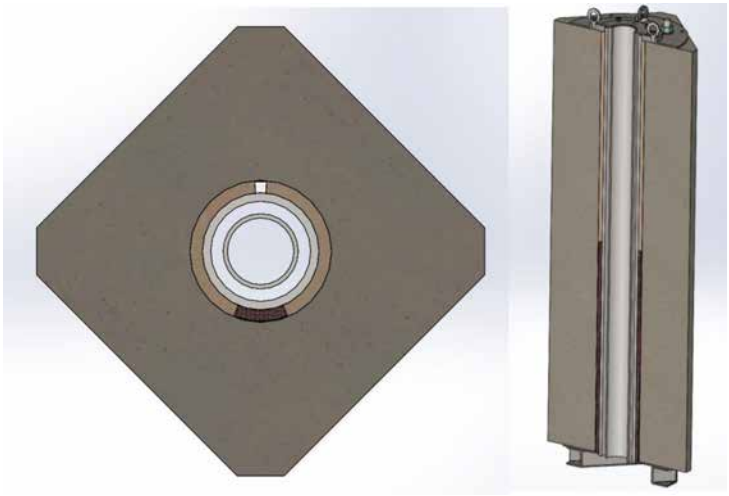


Figure 10—Radial and Axial Cross Sections of the Gamma Test Fixture.

There are 4 different sizes of flaws; 10, 20, 30 and 45 degrees. The top 3 ft has the 10 and 45 degree flaws separated by 180 degrees. The bottom 3 ft section has the 20 and 30 degree flaws again 180 degrees from each other. The bottom flaws are 90 degree offset from the top flaws. In addition, there are 2 short flaws in the bottom section that are extensions of the 10 and 45 degree flaws and they are 6″ long flaws starting from the bottom of the fixture. The cement flaw material is Nylon 12. Its density and effective atomic number are quite similar to those of water. The flaw positioning is shown in Figure 11. Figure 11 shows a picture of the fixture as well.

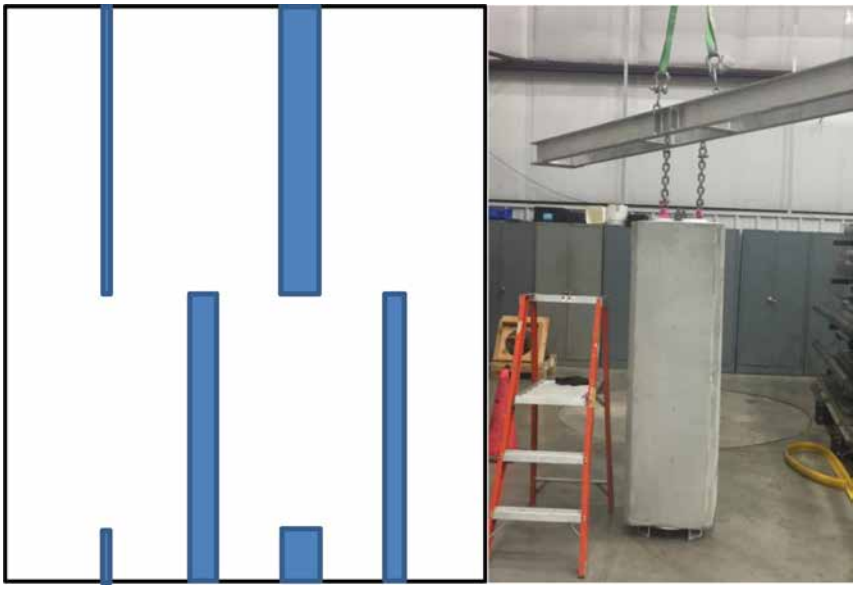


Figure 11—Layout of the Cement Flaws and the Picture of the Test Picture

The second fixture uses a modular approach where there are multiple cores with different flaw structures that can be lowered into a fixed structure. This modular structure is shown in Figure 12. The left drawing shows the structure with the core only where the surrounding formation material is not in place. The right hand side drawing shows the axial cross section that has both the core and the formation material including the rathole. The outer diameter of the cores is 24″. While the completions are similar to the gamma-gamma fixture, the flaw configurations are different. In the first 2 cores, the cement flaws run from bottom to the top. The third core has good cement up to middle section and there is no cement in the higher half of the third core. The fourth core is designed to measure sensitivity to the casing flaws and is quite different than the first three cores. It was produced with a 15 degree cement flaw that goes from the bottom to the top and two casing flaws. One casing flaw is 15 degree wide, 0.12″ deep and goes from 4 ft to 6 ft to the top. The second casing flaw is 30 degree wide, 0.24″ deep and 2ft long from 2ft to 4ft. The second casing flaw is collocated with the cement flaw. Figure 13 shows the pictures of the cores used in this second modular test setup.

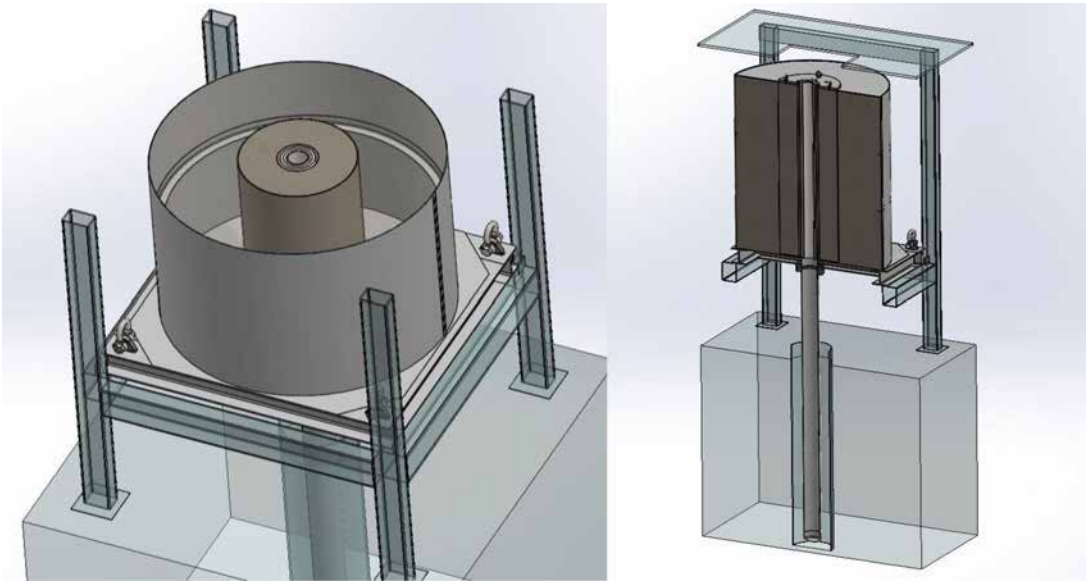


Figure 12—The Drawings of the Modular Fixture and Interchangeable Cores.



Figure 13—Pictures of the Cores Used in the Modular Test Fixture. The Left Shows the First Core Being Lowered into Position. The Right One Shows All of the Cores in a Storage Position.

Experiments

The first set of results are equivalent to right eccentered tubing position shown in Figure 5. The tubing is right eccentered at all positions and the tool face is facing the formation side. This can be seen at the top section of Figure 14. The tool is logged vertically for each of the eight positions and then measurements are stitched together to form the images shown in the second section of Figure 14. The first panel in the second section shows the flaw positions, the second is raw image, the third is interpolated image and the fourth one is filtering applied image. It is very clear that we can see the 20, 30 and 40 degree flaws. The short flaw for 40 degree flaw is visible as well. The relative change in the count rates go up to 30% in this set of results and this is close to what we have observed in the simulation results.

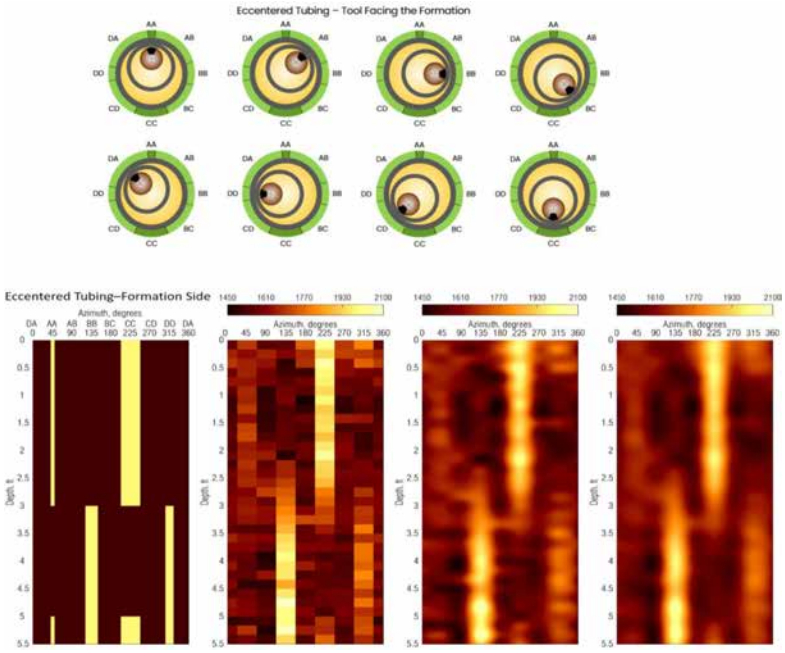


Figure 14—Images Formed from Right Eccentered Measurements.

The second data set is from a centered tubing case. The tubing positioning and the tools in the tubing is shown in the top section of Figure 15. The count rates in this set are higher compared to the set in Figure 14 where the tool face is very close to cement. While the count rates in the right eccentered case were in the 1450-2100 counts/second range, they went up to 2800-4000 counts/second range. This is due to increased distance between the tool face and the cement and occupation of that increased volume by water. As in the previous case, the left most track is the flaw configuration, the second track is raw image, the third track is interpolated image and the last one is filtered image. Although we don't sense the 10 degree flaw at the very left, we can still sense the other flaws.

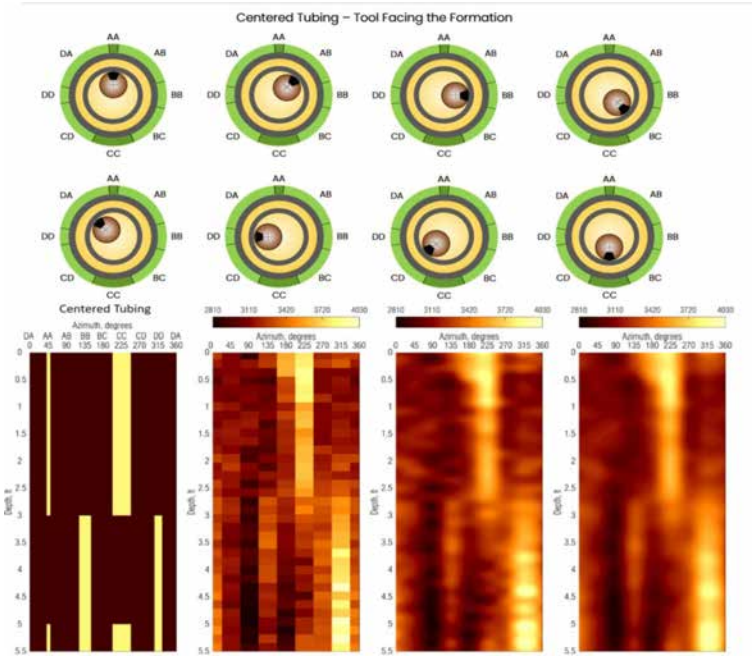


Figure 15—Images Formed from Centered Tubing Measurements.

The third data set is from left centered tubing case. The tubing and tool positioning is shown in the top section of Figure 16. For this case, only four vertical runs were stitched together to form the images. As it is seen in that section, the tool face is quite far from the opposing cement section and that makes this type of measurement the worst case scenario while the right centered tubing shown in Figure 14 is the best case scenario. Due to large water volume between the tool face and the cement section, the count rates are very high and that is due to the low attenuation of gamma rays as discussed in the background section. Although there seems to be some sensitivity to the flaws in the cement, it is relatively low.

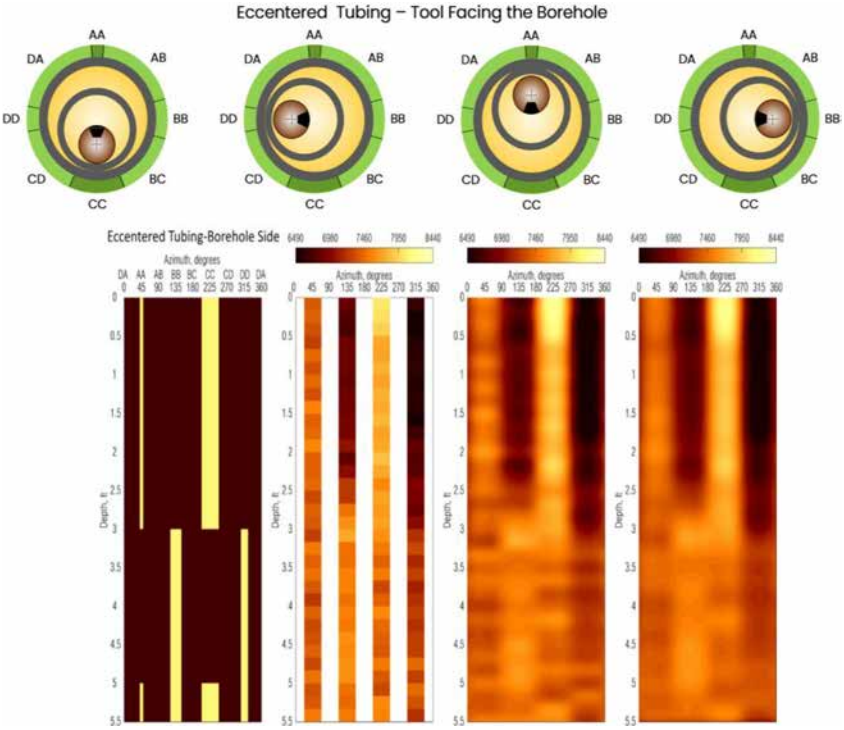


Figure 16—Images Formed from Left Eccentered Tubing Measurements.

The second modular fixture has been used for rotating tool experiments. The change in the volume of water in front of the tool face has a large impact on the measurements. For obtaining a worst case scenario, we conducted these experiments without a tubing in place. This not only increases the distance between the tool face and opposing cement, it also increases the amount of the water significantly. When there is tubing in place, it will force the tool to have a more centralized positioning and reduce the volume of water in front of the tool face. Figure 17 shows some of the positioning used in the experiments.

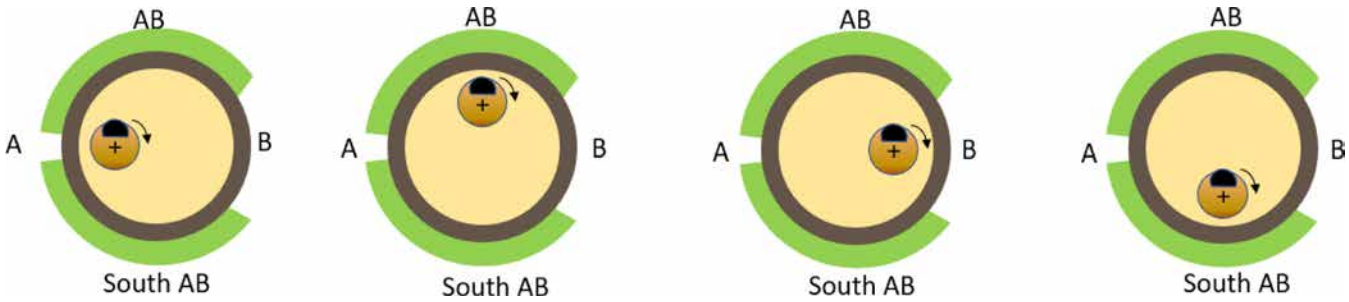


Figure 17—The Tool Positioning in the Rotating Tool Experiments.

The first rotating tool data set is given in Figure 18 and it is based on the tool position A in Figure 17. Although the plots in Figure 17 are given in time domain, they actually represent one full revolution in the

wellbore. At the starting t=0 second point, the tool face is looking upward but the casing is still relatively close to the tool face. Therefore starting count rates we are observing are not very low but not very high either. With tool rotating in clockwise direction, the distance between the tool face and casing increases monotonically till the tool is facing the large flaw B. The count rates follow that trend systematically. Then the count rates start to decrease and when the tool face is pointing at flaw A, the distance between the tool face and the casing is minimum. With that we see a low level count rate plateau from t=35 s to 55 s. Around t=45 s., we also see the flaw signature for the flaw A. The flaw signature is much more visible in the logarithmic plot on the right hand side. One thing that is very different in this plot is we have a sinusoidal background trend created by the water volume varying with the tool rotation. This creates a challenge for such measurements.

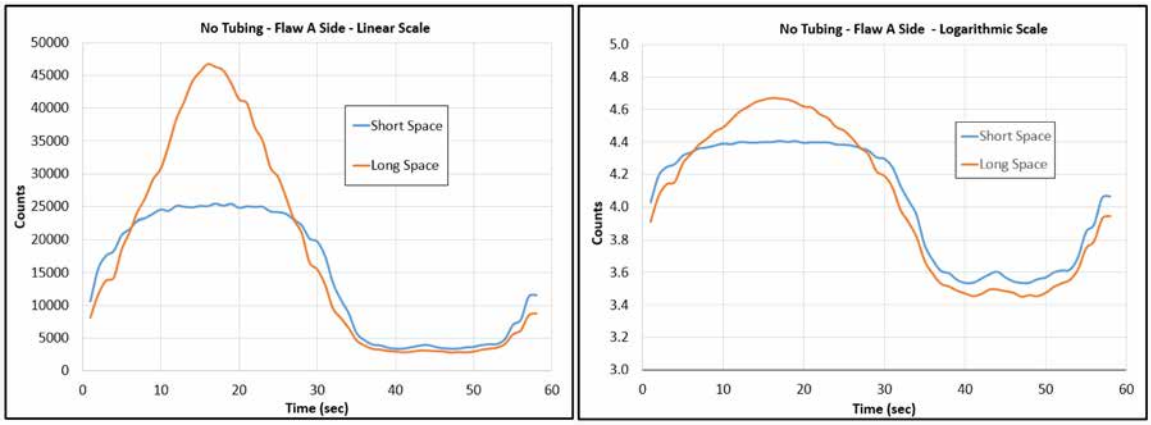


Figure 18—Data from Position A in Figure 17. Left is Linear Scale; Right is Logarithmic Scale.

Figure 19 shows the data collected when the tool is positioned at the south AB position shown in Figure 17. In that position, the tool is relatively distant to both flaws positioned at A and B. So sensitivity to those will be low regardless what the background is. At t=0 second, the tool is facing toward AB position where the water volume is largest. Therefore, starting count rates are at maximum levels. With clockwise rotation, the distance decreases with decreasing count rates and they are at minimum levels from t=13 second to t=22 second when the tool is facing south AB position. After that, the distance starts to increase going back to AB direction again and count rates assume count rates at the starting time. Although the flaws are not noticeable, we see a clear a bump in the count rates around t=5 second which can be attributed to flaw B.

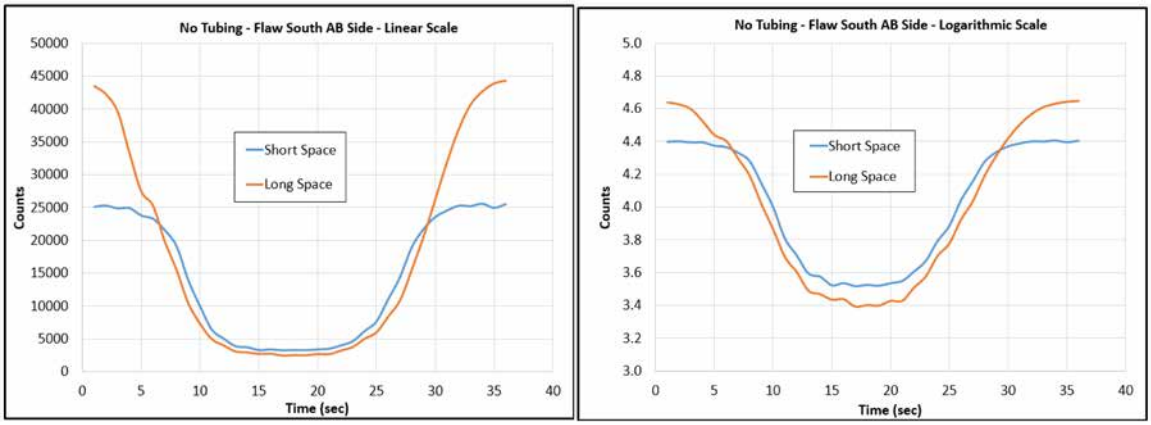


Figure 19—Data from South AB Position in Figure 17.

Figure 20 shows the data taken when the tool is placed near flaw B shown in Figure 17. At the start, the tool is looking north direction but after about 5 seconds, it faces the casing and the distance between the tool face and the casing is the shortest. For similar positions in Figures 18 and 19, the count rates in logarithmic scale are around 3.4. In Figure 20, the matching value is around 3.6. This is most likely due to presence of large amount of water in the cement flaw behind the casing. Although one data point is not enough for a judgment, if it is consistently at that level in an image, it may lead to detection of a flaw. It is difficult to sense the flaw A which is on the other side of the casing due to the distance and the size of the flaw.

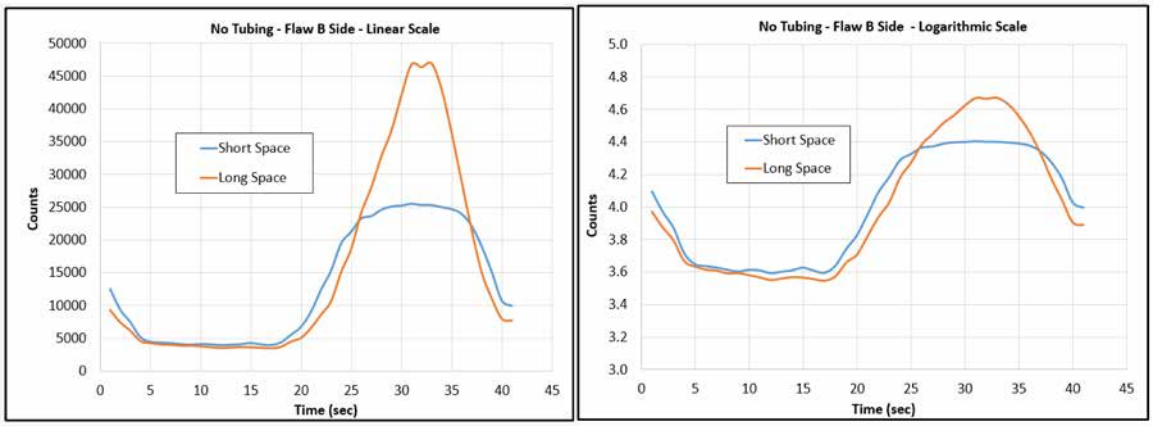


Figure 20—Data from B Position in Figure 17.

The third core in the modular fixture has been designed for testing top of the cement sensitivity. This experiment has been done with the tubing in place but eccentered. The left plot in Figure 21 is for the tool facing the borehole. Due to the large volume of water in front of the tool face, the count rates are very high in this plot. The short space detector does not show any sensitivity. The long space clearly shows an increase from midpoint to the top. The right hand side plot shows the response when the tool faces the formation. Due to closer proximity between the tool face and the cement, the count rates are lower. In this case, it is clear that both short and long space detectors show sensitivity to the top of the cement.

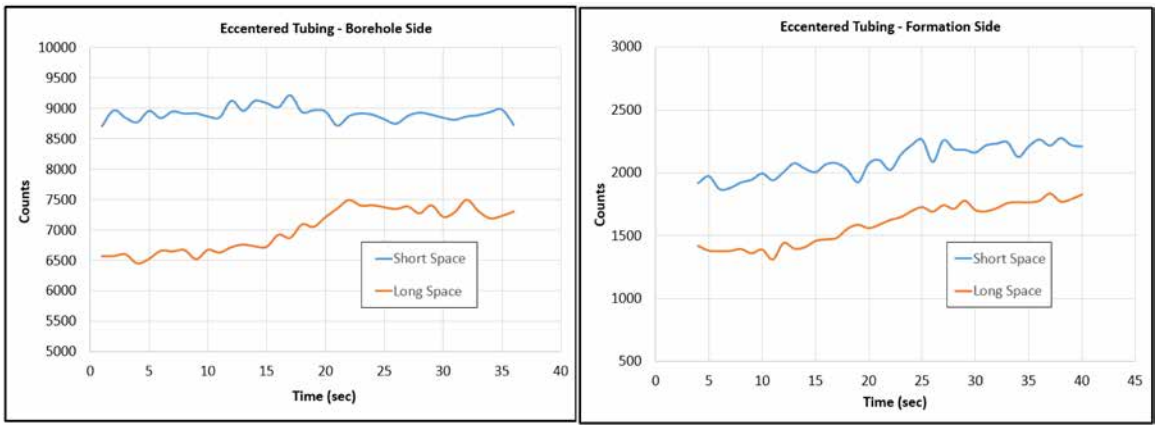


Figure 21—Data from Top of the Cement Sensitivity Measurements.

As discussed in the test fixtures section, the fourth core has a 15 degree casing flaw that extends from 4 ft to 6 ft. The other 30 degree flaw goes from 2 ft to 4 ft. The data seen in the left hand side plot in Figure 22 is for the 15 degree flaw. While the short space detector shows no sensitivity to this flaw, we do see a subtle increasing trend in the long space detector as it gets to that section of the casing. The trends in the right side

plot for 30 degree flaw is more visible. We clearly see an increase in the long space detector count rates in the middle section of the casing. It is clear that there is a sensitivity for the casing flaws as well.

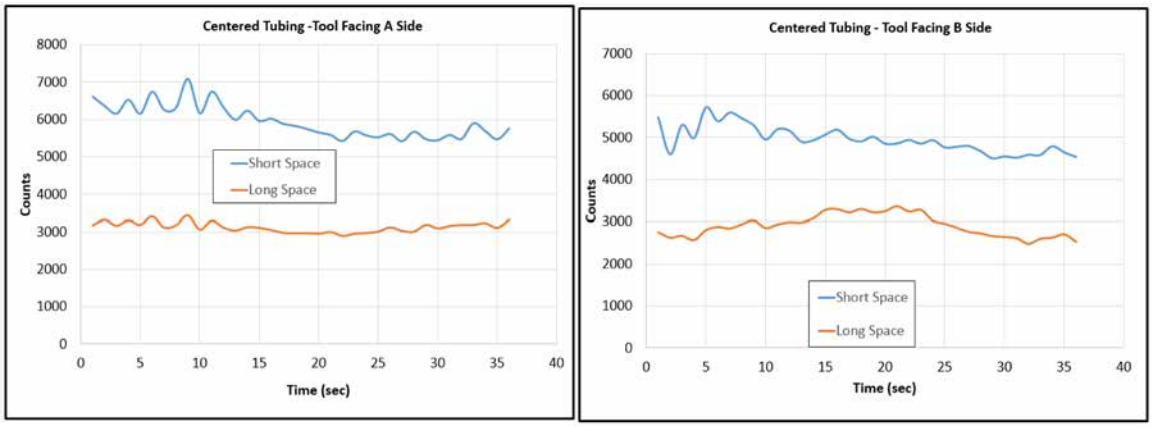


Figure 22—The Response to Casing Flaws.

Conclusions

In this work, we have evaluated the feasibility of using a gamma-gamma measurement principle for detecting cement-based flaws in dual-string completions. Simulations were performed to investigate if the general principles and sensitivity of the proposed measurement strategy warranted future study. The results shown in the Simulations section was deemed to be promising and we pushed forward with experimental validation of the simulation results.

Two fixtures were designed and built to serve as test beds for the experimental logging measurements. The details of these test fixtures were provided. While one is for 3 ft long flaws in a 6 ft long synthetic formation, the other is a modular test fixture that can be used with a set of cores designed to simulate cement flaws, top of the cement and casing flaws. Since the gamma-gamma measurement principle is widely used in existing density measurement tools, we have adapted slick tools from the company inventory to serve as the gamma test articles. The test fixtures and the slick density tool were used in the experiments.

The first set of experiments involved running continuous vertical logs at different azimuthal locations within a tubing that was eccentered at various locations within the borehole. The vertical logging data were stitched together to form 2D images representing counts (pixel intensity) as a function of depth and azimuthal spatial locations. The motivation behind this approach was to determine if the gamma-gamma measurements were showing sensitivity to the cement flaws. Those experiments proved that there is sensitivity to the cement channel flaws greater than 15 degrees, even in the most challenging configurations i.e. when the tool face points toward the borehole and the cement flaws to be detected are very far from the tool face due to the tubing eccentricity. Reconstructed images matched the ideal cement flaw geometries behind casing, both with and without the tubing in place. The relative changes in the count rates were comparable to the relative count rates that we have obtained in the simulations.

The experimental procedure was then repeated on the modular fixture using all the cores build for various scenarios. In this set, the tool has been rotated to have a better understanding of the azimuthal response of the measurements. The experiments conducted in the first two cores showed that there is going to be a sinusoidal background as a function of the tubing eccentricity and this would pose a challenge in identifying some of the signatures. The dynamic range of the data is dominated by the eccentricity of the tubing and tool relative to the fluid within the casing. The maximum-to-minimum count rate ratios were found to be around 15 for extreme cases. This ratio is lower for the centered tubing cases. There appear to be advantages for processing and visualizing the data on a log scale and additional work on the interpretation algorithms is

required. Furthermore, although there is no ability for reducing background signal due to fluid in the annulus between tubing and casing, there is potential for eliminating very high count rates by using a fluid excluder.

This feasibility study shows that this gamma-gamma measurement principle is promising although there are challenges that can be driven by the high level of eccentricity of the tubing positions. This may require development of new image processing methods to mitigate this eccentricity.

Acknowledgments

The authors thank Baker Hughes and TotalEnergies for their support and permission to publish these results.

References

Mwang'ande, Alex William, 2016. Evidences of Poor Cement Displacement Jobs. Master Thesis, Norwegian Institute of Science and Technology.

Fertl, Walter H., Pilkington, Paul E., 1975. Field Tests of Cement Bond Logging Tools. *The Log Analyst* **16** (04).

Gollwitzer, L. H., Masson, J. P., 1982. The Cement Bond Tool. *SPWLA 23rd Annual Logging Symposium*.

Hawtorn, A,Steinsiek, R,Rahman, Shaela, 2022. Casing and Cement Evaluation on Drillpipe : New Tool Acquires Well Integrity Data in Parallel with Existing Drillpipe Deployed Operations from Drilling to Plug and Abandonment. Kuala Lumpur, Malaysia, OTC-31502-MS.

Moake, G. L., 1998. Design of a Cased-Hole-Density Logging Tool Using Laboratory Measurements. New Orleans, Lousiana, SPE 49226.

Ellis, Drawing, Luling, Martin G, Markley, Marvin E, et al. 2004. Cased-Hole Formation-Density Logging – Some Field Experiences. *SPWLA 45th Annual Logggins Symposium*, Paper G.

Li, Yulian, Qiong, Zhang, Jin, Ya, et al. 2022. A Novel Interpretation Model for Cased Hole Density Measurement. *SPWLA 63th Annual Logging Symposium*, Stavenger, Norway.

Kasten, M, Mandal S, Ross, W, et al. 2016 Multi-Casing Well Integrity Inspection in Oil and Gas Wells. Midland, Texas, SPE-181776-MS.

Hu, Yike, Guo, Weijun, 2016. Behind Casing Inspection Using Active Gamma-Gamma Technique. Kula Lumpur, Malaysia, OTC-26639-MS.

Inanc, Feyzi, Yuan Peng, Ramirez, Marc and Jones, Allan. 2021. System and Method for a Downhole Gamma Ray Instrument. US 11,067,716 B2.

XCOM: Photon Cross Section Database (version 1.5). [Online] Available: http://physics.nist.gov/xcom [2022, May 27]. National Institute of Standards and Technology, Gaithersburg, MD, 2010.

C.J. Werner, et al, "MCNP6. 2 Release Notes", Los Alamos National Laboratory, report LA-UR-18-20808 (2018)